Higher-order rogue wave solutions of the three-wave resonant interaction equation via the generalized Darboux transformation

IOP Publishing | Royal Swedish Academy of Sciences Physica Scripta

Phys. Scr. 90 (2015) 105201 (12pp) doi:10.1088/0031-8949/90/10/105201

Higher-order rogue wave solutions of the three-wave resonant interaction equation via the generalized Darboux transformation

Xin Wang[1], Jianli Cao[2] and Yong Chen[1]

[1] Shanghai Key Laboratory of Trustworthy Computing, East China Normal University, Shanghai, 200062, People's Republic of China
[2] College of Science, Henan University of Technology, Zhengzhou, Henan, 450001, People's Republic of China

E-mail: ychen@sei.ecnu.edu.cn

Received 5 February 2015, revised 28 July 2015
Accepted for publication 7 August 2015
Published 18 September 2015

Abstract

In this paper, we utilize generalized Darboux transformation to study higher-order rogue wave solutions of the three-wave resonant interaction equation, which describes the propagation and mixing of waves with different frequencies in weakly nonlinear dispersive media. A general Nth-order rogue wave solution with two characteristic velocities structural parameters and $3N$ independent parameters under a determined plane-wave background and a specific parameter condition is derived. As an application, we show that four fundamental rogue waves with fundamental, two kinds of line and quadrilateral patterns, or six fundamental rogue waves with fundamental, triangular, two kinds of quadrilateral and circular patterns can emerge in the second-order rogue waves. Moreover, several important wave characteristics including the maximum values, the corresponding coordinate positions of the humps, and the stability problem for some special higher-order rogue wave solutions such as the fundamental and quadrilateral cases are discussed.

Keywords: rogue wave, generalized Darboux transformation, three-wave resonant interaction equation

(Some figures may appear in colour only in the online journal)

1. Introduction

Rogue waves (or freak waves and a number of other similar names) originally being used to describe short-lived gigantic surface gravity waves in the deep ocean [1], have received an unprecedented surge of research activities in many realms of science within the last few years, optical fibers [2], mode-locked lasers [3], Bose–Einstein condensates [4], to name a few. Compared to solitons and breathers, rogue waves are localized in both space and time, and they suddenly come from nowhere and instantaneously vanish without a trace [5]. Mathematically, a single rogue wave is formally described by the well-known Peregrine soliton, a prototypical solution of the scalar nonlinear Schrödinger (NLS) equation, which is expressed by the rational polynomials of second order, and its maximum value is three times greater than the average state [6]. Moreover, rogue waves have been experimentally observed in a water wave tank [7, 8], etc.

Recent studies on rogue waves are rapidly concentrated on multi-component coupled systems, since the scalar models cannot depict the essential interaction processes among the nonlinear waves with different modes or frequencies [9]. One of the most famous coupled models is the Manakov system, which serves as basic equations to depict the light wave transmission in birefringent optical fibres, and to simulate the crossing sea waves in deep ocean [10]. This system follows the weak resonant condition, and it is accepted that dark rogue waves [11], the interaction between rogue waves and solitons or breathers [9, 12], composite rogue waves [11, 13] and four-petaled rogue waves [14] can all exist in it. While when considering the extreme waves in strong resonant processes, the three-wave resonant interaction (TWRI) equation is of fundamental and universal significance [15].

In this paper, we choose to consider the following general three coupled system [16]

$$\begin{aligned} u_{1t} + c_1 u_{1x} &= u_3^* u_2, \\ u_{2t} + c_2 u_{2x} &= -u_3 u_1, \\ u_{3x} + (c_1 - c_2) u_1^* u_2 &= 0, \end{aligned} \tag{1}$$

where u_1, u_2 and u_3 are three complex envelops of waves, c_1 and c_2 being assumed to satisfy the ordering condition $0 < c_1 < c_2$ define the characteristic velocities. The subscripts represent the partials and the asterisk delegates the complex conjugation. This general system models the nonlocal interaction of two waves if t is the evolution variable, and models the TWRI if x is the evolution variable. In this paper, we assume x to be the evolution variable, and t is the second independent variable. For concrete physical contexts, equation (1) can describe the propagation and mixing of waves with different frequencies in weakly nonlinear dispersive media [15, 16], and it is of also elementary application in nonlinear optics [17], fluid dynamics [18], plasma physics [19], solid state physics [20], and so forth. Over recent years, there have been a substantial number of reports for equation (1), such as the inverse scattering transformation studied by Kaup [17], the Darboux transformation (DT) and multi-soliton solutions given by Zhou [21], and the finite dimensional Hamiltonian system and algebro-geometric solutions derived by Geng and Wu *et al* [22, 23]. Especially, in recent years, by using the Darboux-dressing method and spectral techniques, the general soliton solutions, lower-order rogue wave solutions and stability problem of the solutions have been systematically investigated by Degasperis, Baronio, Conforti *et al* [15, 16, 24, 25]. However, to our knowledge, there are no reports on higher-order rogue wave solutions of the general three-coupled system (1).

As a matter of fact, higher-order rogue waves can be viewed as the nonlinear superposition of a certain amount of fundamental rogue waves, and they can be described by the complicated higher-order rational polynomials instead of the simple Peregrine soliton. Very recently, higher-order rogue waves of the scalar NLS equation have been successfully generated in a water wave tank, which gives a definitive answer of the theoretical predictions of their existence [26]. Also, the complete classification of the higher-order rogue wave solutions for the scalar NLS equation have been presented in [27, 28]. Nevertheless, as far as we know, there is relatively scarce literature about higher-order rogue wave solutions of the coupled systems due to their complexity and variousness. Fortunately, under the integrability condition [29, 30], the generalized DT method developed by Ling [13] provide an effective way to solve this problem [31–37].

In this paper, based on the determined plane-wave background and a specific spectral condition, we derive a general Nth-order rogue wave solution of direct iterative rule and its equivalent $3N \times 3N$ degree determinant form for equation (1) by using the generalized DT method. The general solution contains two characteristic velocities structural parameters and $3N$ independent parameters. Particularly, by means of the symbolic computation [38, 39], for $N = 1$, the explicit first-order rogue wave solution containing polynomials of second order or fourth order is just the rogue wave solution with respect to the triple root case of $q = \frac{1}{2}$ given in [16]. For $N = 2$, the second-order rogue wave solution consisting of polynomials of eighth or twelfth order is obtained. We show that the second-order rogue waves including fundamental, two kinds of line and quadrilateral patterns can be obtained, the corresponding expressions of the solutions are related to eighth-order polynomials. Furthermore, it is shown that six fundamental rogue waves with fundamental, triangular, two kinds of quadrilateral and circular patterns can emerge in the second-order rogue waves, the solutions can be expressed by twelfth-order polynomials. Some significant wave characteristics including the maximum amplitudes and the corresponding coordinate positions of the humps in the higher-order rogue waves are calculated. We numerically show that with the composite numbers of the fundamental rogue waves increasing, the corresponding maximum amplitudes of the humps in the higher-order rogue waves are amplified. Also, the stability problem [40] of some special higher-order rogue waves is discussed.

The paper is organized as follows. In section 2, we derive the generalized DT and a general Nth-order rogue wave solution of the TWRI equation. In section 3, some explicit rogue wave solutions and their numerical plots are shown. The last section is the conclusion.

2. General Nth-order rogue wave solution

In this section, we shall construct a general Nth-order rogue wave solution for equation (1), which can be represented by the compatibility condition of following Lax pair

$$\Psi_x = U\Psi, \quad U = \mathrm{i}\zeta\sigma + U_0, \tag{2}$$

$$\Psi_t = V\Psi, \quad V = 2\mathrm{i}\zeta C - \sigma V_0 + \sigma\left[C, U_0\right], \tag{3}$$

where

$$U_0 = \begin{pmatrix} 0 & -u_1^* & -u_2^* \\ u_1 & 0 & 0 \\ u_2 & 0 & 0 \end{pmatrix}, \quad V_0 = \begin{pmatrix} 0 & 0 & 0 \\ 0 & 0 & u_3^* \\ 0 & -u_3 & 0 \end{pmatrix},$$

$\sigma = \mathrm{diag}\{1, -1, -1\}$ and $C = \mathrm{diag}\{0, c_1, c_2\}$. Here $\Psi = (\psi(x, t), \phi(x, t), \chi(x, t))^{\mathrm{T}}$ is the eigenfunction and ζ is the spectral parameter.

Next, let $\Psi_1 = (\psi_1, \phi_1, \chi_1)^{\mathrm{T}}$ be a basic solution of the spectral problem (2) and (3) with $u_1 = u_1[0]$, $u_2 = u_2[0]$, $u_3 = u_3[0]$ and $\zeta = \zeta_1$, then the classical DT of the spectral problem (2) and (3) holds

$$\Psi[1] = T[1]\Psi, \, T[1] = \zeta I - H[0]\Lambda_1 H[0]^{-1}, \tag{4}$$

$$\begin{aligned} u_1[1] = u_1[0] &+ 2\mathrm{i}\left(\zeta_1^* - \zeta_1\right) \\ &\times \frac{\psi_1[0]^* \phi_1[0]}{\left(\left|\psi_1[0]\right|^2 + \left|\phi_1[0]\right|^2 + \left|\chi_1[0]\right|^2\right)}, \end{aligned} \tag{5}$$

$$\begin{aligned} u_2[1] = u_2[0] &+ 2\mathrm{i}\left(\zeta_1^* - \zeta_1\right) \\ &\times \frac{\psi_1[0]^* \chi_1[0]}{\left(\left|\psi_1[0]\right|^2 + \left|\phi_1[0]\right|^2 + \left|\chi_1[0]\right|^2\right)}, \end{aligned} \tag{6}$$

$$u_3[1] = u_3[0] + 2\mathrm{i}(c_1 - c_2)\left(\zeta_1 - \zeta_1^*\right) \frac{\phi_1[0]^*\chi_1[0]}{\times\left(\left|\psi_1[0]\right|^2 + \left|\phi_1[0]\right|^2 + \left|\chi_1[0]\right|^2\right)}, \quad (7)$$

where $(\psi_1[0], \phi_1[0], \chi_1[0])^{\mathsf{T}} = (\psi_1, \phi_1, \chi_1)^{\mathsf{T}} = \Psi_1[0]$, I is the 3×3 identity matrix,

$$H[0] = \begin{pmatrix} \psi_1[0] & \phi_1[0]^* & \chi_1[0]^* \\ \phi_1[0] & -\psi_1[0]^* & 0 \\ \chi_1[0] & 0 & -\psi_1[0]^* \end{pmatrix}, \quad \Lambda_1 = \begin{pmatrix} \zeta_1 & 0 & 0 \\ 0 & \zeta_1^* & 0 \\ 0 & 0 & \zeta_1^* \end{pmatrix}.$$

Now given that $\Psi_1 = \Psi_1(\zeta_1 + \delta)$ is a special solution of the spectral problem (2) and (3) under the initial condition $u_1 = u_1[0], u_2 = u_2[0], u_3 = u_3[0]$ and $\zeta = \zeta_1 + \delta$, and it can be expanded as the Taylor series

$$\Psi_1 = \Psi_1^{[0]} + \Psi_1^{[1]}\delta + \Psi_1^{[2]}\delta^2 + \cdots + \Psi_1^{[N-1]}\delta^{N-1} + \cdots, \quad (8)$$

here δ is a small parameter, $\Psi_1^{[j]} = (\psi_1^{[j]}, \phi_1^{[j]}, \chi_1^{[j]}) = \frac{1}{j!}\frac{\partial^j}{\partial\delta^j}\,|_{\delta\to 0}\,\Psi_1 (j = 0, 1, 2, \ldots)$.

At this time, it follows from the classical DT (4)–(7) that the N-step generalized DT can be constructed as follows.

$$\begin{aligned} \Psi_1[N-1] &= \Psi_1^{[0]} + \sum_{l=1}^{N-1} T_1[l]\Psi_1^{[1]} \\ &\quad + \sum_{l=1}^{N-1}\sum_{k=1}^{l-1} T_1[l]T_1[k]\Psi_1^{[2]} \\ &\quad + \cdots + T_1[N-1]T_1[N-2]\cdots T_1[1]\Psi_1^{[N-1]}, \\ \Psi[N] &= T[N]T[N-1]\cdots T[1]\Psi,\ T[l] \\ &= \zeta I - H[l-1]\Lambda_l H[l-1]^{-1}, \end{aligned} \quad (9)$$

$$u_1[N] = u_1[0] + 2\mathrm{i}\left(\zeta_1^* - \zeta_1\right) \times \sum_{l=1}^{N} \frac{\psi_1[l-1]^*\phi_1[l-1]}{\left(\left|\psi_1[l-1]\right|^2 + \left|\phi_1[l-1]\right|^2 + \left|\chi_1[l-1]\right|^2\right)}, \quad (10)$$

$$u_2[N] = u_2[0] + 2\mathrm{i}\left(\zeta_1^* - \zeta_1\right) \times \sum_{l=1}^{N} \frac{\psi_1[l-1]^*\chi_1[l-1]}{\left(\left|\psi_1[l-1]\right|^2 + \left|\phi_1[l-1]\right|^2 + \left|\chi_1[l-1]\right|^2\right)}, \quad (11)$$

$$u_3[N] = u_3[0] + 2\mathrm{i}(c_1 - c_2)\left(\zeta_1 - \zeta_1^*\right) \times \sum_{l=1}^{N} \frac{\phi_1[l-1]^*\chi_1[l-1]}{\left(\left|\psi_1[l-1]\right|^2 + \left|\phi_1[l-1]\right|^2 + \left|\chi_1[l-1]\right|^2\right)}, \quad (12)$$

where

$$H[l-1] = \begin{pmatrix} \psi_1[l-1] & \phi_1[l-1]^* & \chi_1[l-1]^* \\ \phi_1[l-1] & -\psi_1[l-1]^* & 0 \\ \chi_1[l-1] & 0 & -\psi_1[l-1]^* \end{pmatrix},$$

$$\Lambda_l = \begin{pmatrix} \zeta_1 & 0 & 0 \\ 0 & \zeta_1^* & 0 \\ 0 & 0 & \zeta_1^* \end{pmatrix}.$$

In addition, let us define

$$\Psi_1^{[j,m]} = \frac{1}{m!}\frac{\partial}{\partial\delta^m}\,|_{\delta\to 0}\left(\zeta_1 + \delta\right)^j\Psi_1, \quad j = 0, 1, \ldots, N,\ m = 0, 1, \ldots, N-1, \quad (13)$$

then the formulas (10)–(12) can be written as the $3N \times 3N$ degree determinant form, which is just the general Nth-order rogue wave solution for equation (1), i.e.

$$u_1[N] = u_1[0] + 2\mathrm{i}\frac{\det(M_1)}{\det(M)}, \quad (14)$$

$$u_2[N] = u_2[0] + 2\mathrm{i}\frac{\det(M_2)}{\det(M)}, \quad (15)$$

$$u_3[N] = u_3[0] + 2\mathrm{i}(c_2 - c_1)\frac{\det(M_3)}{\det(M)}, \quad (16)$$

where

$$M = \begin{pmatrix} \psi_1^{[N-1,0]} & \phi_1^{[N-1,0]} & \chi_1^{[N-1,0]} \\ \phi_1^{[N-1,0]*} & -\psi_1^{[N-1,0]*} & 0 \\ \chi_1^{[N-1,0]*} & 0 & -\psi_1^{[N-1,0]*} \\ \psi_1^{[N-1,1]} & \phi_1^{[N-1,1]} & \chi_1^{[N-1,1]} \\ \phi_1^{[N-1,1]*} & -\psi_1^{[N-1,1]*} & 0 \\ \chi_1^{[N-1,1]*} & 0 & -\psi_1^{[N-1,1]*} \\ \cdots & \cdots & \cdots \\ \psi_1^{[N-1,N-1]} & \phi_1^{[N-1,N-1]} & \chi_1^{[N-1,N-1]} \\ \phi_1^{[N-1,N-1]*} & -\psi_1^{[N-1,N-1]*} & 0 \\ \chi_1^{[N-1,N-1]*} & 0 & -\psi_1^{[N-1,N-1]*} \\ \psi_1^{[N-2,0]} & \phi_1^{[N-2,0]} & \chi_1^{[N-2,0]} \\ \phi_1^{[N-2,0]*} & -\psi_1^{[N-2,0]*} & 0 \\ \chi_1^{[N-2,0]*} & 0 & -\psi_1^{[N-2,0]*} \\ \psi_1^{[N-2,1]} & \phi_1^{[N-2,1]} & \chi_1^{[N-2,1]} \\ \phi_1^{[N-2,1]*} & -\psi_1^{[N-2,1]*} & 0 \\ \chi_1^{[N-2,1]*} & 0 & -\psi_1^{[N-2,1]*} \\ \cdots & \cdots & \cdots \\ \psi_1^{[N-2,N-1]} & \phi_1^{[N-2,N-1]} & \chi_1^{[N-2,N-1]} \\ \phi_1^{[N-2,N-1]*} & -\psi_1^{[N-2,N-1]*} & 0 \\ \chi_1^{[N-2,N-1]*} & 0 & -\psi_1^{[N-2,N-1]*} \\ \cdots & \psi_1^{[0,0]} & \phi_1^{[0,0]} & \chi_1^{[0,0]} \\ \cdots & \phi_1^{[0,0]*} & -\psi_1^{[0,0]*} & 0 \\ \cdots & \chi_1^{[0,0]*} & 0 & -\psi_1^{[0,0]*} \\ \cdots & \psi_1^{[0,1]} & \phi_1^{[0,1]} & \chi_1^{[0,1]} \\ \cdots & \phi_1^{[0,1]*} & -\psi_1^{[0,1]*} & 0 \\ \cdots & \chi_1^{[0,1]*} & 0 & -\psi_1^{[0,1]*} \\ \cdots & \cdots & \cdots & \cdots \\ \cdots & \psi_1^{[0,N-1]} & \phi_1^{[0,N-1]} & \chi_1^{[0,N-1]} \\ \cdots & \chi_1^{[0,N-1]*} & 0 & -\psi_1^{[0,N-1]*} \end{pmatrix}$$

M_1 is M with the first column replaced by L_1,

$$L_1 = \left(-\phi_1^{[N,0]}, \psi_1^{[N,0]*}, 0, -\phi_1^{[N,1]}, \psi_1^{[N,1]*}, 0, \cdots, -\phi_1^{[N,N-1]}, \psi_1^{[N,N-1]*}, 0\right)^{\mathsf{T}},$$

M_2 and M_3 are M with the first and second column replaced by L_2, respectively,

$$L_2 = \left(-\chi_1^{[N,0]}, 0, \psi_1^{[N,0]*}, -\chi_1^{[N,1]}, 0, \psi_1^{[N,1]*}, \cdots, -\chi_1^{[N,N-1]}, 0, \psi_1^{[N,N-1]*}\right)^{T}.$$

3. Dynamics of the higher-order rogue wave solutions

In this section, we try to obtain the explicit rogue wave solution for equation (1) by using the generalized DT. Here, we begin with the following plane-wave solution

$$u_1[0] = \exp\left[\mathrm{i}\theta_1\right], \quad u_2[0] = \exp\left[\mathrm{i}\theta_2\right],$$
$$u_3[0] = \mathrm{i}(c_2 - c_1)\exp\left[\mathrm{i}\theta_3\right], \tag{17}$$

where

$$\theta_1 = \frac{1}{2}x + \left(\frac{c_1}{2} - c_2\right)t,$$
$$\theta_2 = -\frac{1}{2}x + \left(c_1 - \frac{c_2}{2}\right)t,$$
$$\theta_3 = -x + \frac{(c_1 + c_2)}{2}t.$$

Then substituting (17) into the spectral problem (2) and (3) under the spectral parameter condition

$$\zeta = \zeta_1\left(1 + \theta^3\right) = \frac{3}{4}\sqrt{3}\,\mathrm{i}\left(1 + \theta^3\right), \tag{18}$$

we have the following basic solution matrix taking the form of

$$S(\theta) = G\left(S_1, S_2, S_3\right), \tag{19}$$

where

$$G = \begin{pmatrix} 1 & 0 & 0 \\ 0 & \exp\left[\mathrm{i}\theta_1\right] & 0 \\ 0 & 0 & \exp\left[\mathrm{i}\theta_2\right] \end{pmatrix},$$

$$S_i = \begin{pmatrix} \left[\mathrm{i}\left(\zeta - \frac{1}{2}\right) + \xi_i\right]\left[\mathrm{i}\left(\zeta + \frac{1}{2}\right) + \xi_i\right]\exp[\omega_i] \\ \left[\mathrm{i}\left(\zeta - \frac{1}{2}\right) + \xi_i\right]\exp[\omega_i] \\ \left[\mathrm{i}\left(\zeta + \frac{1}{2}\right) + \xi_i\right]\exp[\omega_i] \end{pmatrix},$$

$i = 1, 2, 3,$

with

$$\omega_i = \xi_i x + \left[\mathrm{i}(c_2 - c_1)\xi_i^2 - \frac{(c_1 + c_2)}{2}\xi_i + \left(\mathrm{i}(c_2 - c_1)\zeta^2 + \frac{1}{2}\mathrm{i}(c_1 + c_2)\zeta - 2\mathrm{i}(c_1 - c_2)\right)\right]t,$$

and ξ_i satisfies a cubic algebraic equation

$$\xi^3 - \frac{3}{4}\sqrt{3}\left(\theta^3 + 1\right)\xi^2 - \frac{9}{16}\left(3\theta^6 + 6\theta^3 - 1\right)\xi + \frac{3}{64}\sqrt{3}\left(27\theta^9 + 81\theta^6 + 53\theta^3 - 1\right) = 0, \tag{20}$$

here θ is a small parameter, and when by setting $\theta \to 0$, it is easy to calculate that the above cubic algebraic equation (20) possesses a triple roots, that is, $\xi_1 = \xi_2 = \xi_3 = \frac{\sqrt{3}}{4}$.

Then, in order to obtain an adequate solution of the spectral problem (2) and (3) under initial condition (17) and (18), we define

$$\Psi_1(\theta) = f\Psi_{11} + g\Psi_{12} + h\Psi_{13}, \tag{21}$$

where

$$f = \sum_{k=1}^{N} f_k \theta^{3(k-1)},$$
$$g = \sum_{k=1}^{N} g_k \theta^{3(k-1)},$$
$$h = \sum_{k=1}^{N} h_k \theta^{3(k-1)},$$

and

$$\Psi_{11} = \frac{2}{3}\left(S_1 + S_2 + S_3\right),$$
$$\Psi_{12} = \frac{2}{3}\sqrt[3]{2}\left(\frac{S_1}{\theta} - a\frac{S_2}{\theta} - a^*\frac{S_3}{\theta}\right),$$
$$\Psi_{13} = \frac{4}{3}\sqrt[3]{4}\left(\frac{S_1}{\theta^2} - a^*\frac{S_2}{\theta^2} - a\frac{S_3}{\theta^2}\right),$$

with $a = \exp[\mathrm{i}\pi/3]$ and f_k, g_k, h_k $(1 \leqslant k \leqslant N)$ are $3N$ real independent constants.

At this moment, we note that $\Psi_1(\theta)$ given by (21) can be expanded around $\theta = 0$ with the form

$$\Psi_1(\theta) = \Psi_1^{[0]} + \Psi_1^{[1]}\theta^3 + \Psi_1^{[2]}\theta^6 + \cdots + \Psi_1^{[N-1]}\theta^{3(N-1)} + O\left(\theta^{3N}\right), \tag{22}$$

where $\Psi_1^{[j]} = (\psi_1^{[j]}, \phi_1^{[j]}, \chi_1^{[j]})^{\mathsf{T}} = \frac{1}{3j!}\frac{\partial^{3j}}{\partial\theta^{3j}}|_{\theta\to 0}\,\Psi_1(\theta)$, $j = 0, 1, 2, \ldots$, and the complicated expressions are omitted in this paper.

Hereby, we only need to adjust the definition of (13) by

$$\Psi_1^{[j,m]} = \frac{1}{3\,m!}\frac{\partial}{\partial\theta^{3\,m}}|_{\theta\to 0}\left(\zeta_1\left(1 + \theta^3\right)\right)^j\Psi_1(\theta),$$
$$j = 0, 1, \ldots, N,$$
$$m = 0, 1, \ldots, N - 1, \tag{23}$$

then a series of rogue wave solutions of equation (1) can be derived by the formulas (14)–(16).

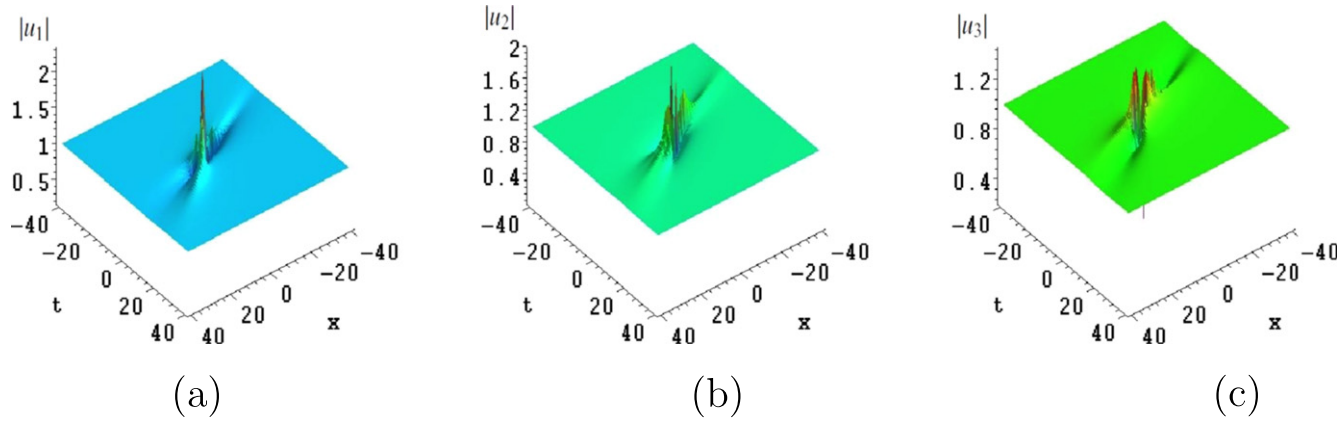

Figure 1. Evolution plot of the second-order rogue waves of fundamental pattern with $c_1 = 1$, $c_2 = 2$, $f_1 = 0$, $g_1 = 1$, $h_1 = 0$, $f_2 = 0$, $g_2 = 0$, $h_2 = 0$.

For $N = 1$, we arrive at the first-order rogue wave solution with two characteristic velocities structural parameters c_1 and c_2 and three independent parameters, namely, f_1, g_1, h_1. For $N = 2$, the second-order rogue wave solution involving two characteristic velocities structural parameters c_1 and c_2 and six independent parameters, i.e. f_k, g_k, h_k ($k = 1, 2$) is obtained. Now we classify dynamics of the second-order rogue wave solution into two cases via the essential parameter h_1 be zero or not.

Case 1 $h_1 = 0$. At this point, it is calculated that the solution consists of polynomials of eighth order rather than the simple second or fourth order. In the next, for convenience, we omit presenting the concrete expressions of the higher-order solutions for they can be directly derived by the determinant formulas (14)–(16) and (23) through choosing different free parameters.

Now when choosing $g_1 \neq 0$ and the other free parameters be zero, the fundamental higher-order rogue wave which is featured by a composite of four fundamental rogue waves merged with each other is obtained, see figures 1(a)–(c). Through numerical calculation, we find that the interaction process can enhance the maximum amplitude of the humps, when four fundamental rogue waves intermingle with each other, the maximum value can reach to four times greater than the background crest. In addition, it is explicitly computed that the maximum amplitudes of the humps in u_1 component are equal to that in u_2 component, while in u_3 component the values are different. The concrete numerical data including maximum amplitudes and the corresponding coordinate positions of the humps are shown in table 1.

When taking $g_1 \neq 0$, $h_2 \neq 0$, it is exhibited that in figures 2(a)–(c), two fundamental rogue waves on either hand, together with a new rogue wave which is formed by the interaction of two fundamental ones in the middle distribute with a line (line pattern 1) on the temporal-spacial plane; when letting $g_1 \neq 0$, $f_1 \neq 0$, we display that in figures 3(a)–(c), a new rogue wave which is constituted by the interaction of two fundamental ones localizes around the origin (0, 0), along with two fundamental rogue waves distributing in the x-axis positive direction, and we call this dynamical structure as the line pattern 2; while when choosing $g_1 \neq 0$, $f_2 \neq 0$, a composite of four well-separated fundamental rogue waves arranging with a quadrilateral can be exhibited, see figures 4(a)–(c). Here, it should be pointed out that comparing to the rhombus and rectangle pattern in the Manakov system, rogue waves over here would be tilted significantly to spread like a parallelogram pattern. The temporal-spacial distributions in u_1, u_2 and u_3 components are globally similar, but the concrete maximum amplitudes, temporal appearance and spacial localization of the humps in each component may be different. For u_1 component, the maximum amplitudes of the four humps are 2.1181, 1.9176, 2.0621 and 1.8702, and occur at (20.4318,13.2336), (13.4873,0.1596), (−9.8754, −0.0079) and (−19.0444, −13.0172), respectively. For u_2 component, the maximum amplitudes are entirely the same as u_1 component, while the corresponding coordinate positions are (−19.2692, −13.2336), (13.0084, −0.1596), (−9.8518, 0.0079) and (20.0072, 13.0172), respectively. For u_3 component, the maximum values are different from the aforementioned components, they are 2.0207, 2.1706, 1.8821 and 2.0207, and arrive at (20.4333, 13.2330), (13.3449,0), (−10.0703, 0) and (−19.2657, −13.2330), respectively.

Case 2 $h_1 \neq 0$. At this moment, the solution is made up of polynomials of twelfth order, and we will see that six fundamental rogue waves can coexist in the second-order rogue waves of equation (1), which is similar to the third-order rogue waves with triangular or circular pattern in the scalar NLS equation. Nevertheless, we would like to remark that dynamical structures of rogue waves over here are much more abundant than that in the scalar model due to the existence of the multiple independent parameters.

Here, we find that dynamical structures of the higher-order rogue waves in this case can be classified into five types. By letting $h_1 \neq 0$ and the other independent parameters be zero, the fundamental pattern which is featured by a composite of six fundamental rogue waves intermingled with each other is presented, see figures 5(a)–(c). Though numerical computation, we find that when six fundamental rogue waves in equation (1) merge with each other, the maximum amplitude of the humps run up to almost five times larger than the average value. Furthermore, we present that the maximum amplitudes of the humps at this time in u_1 component are also

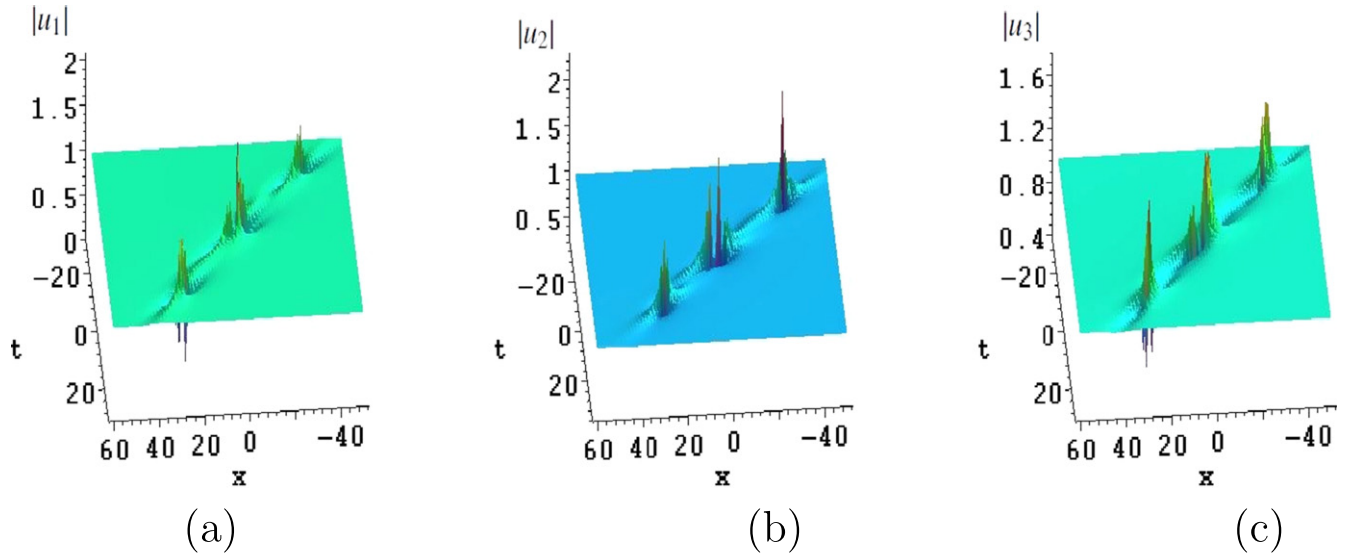

Figure 2. Evolution plot of the second-order rogue waves of line pattern 1 with $c_1 = 1, c_2 = 2, f_1 = 0, g_1 = 1, h_1 = 0, f_2 = 0, g_2 = 0, h_2 = 50$.

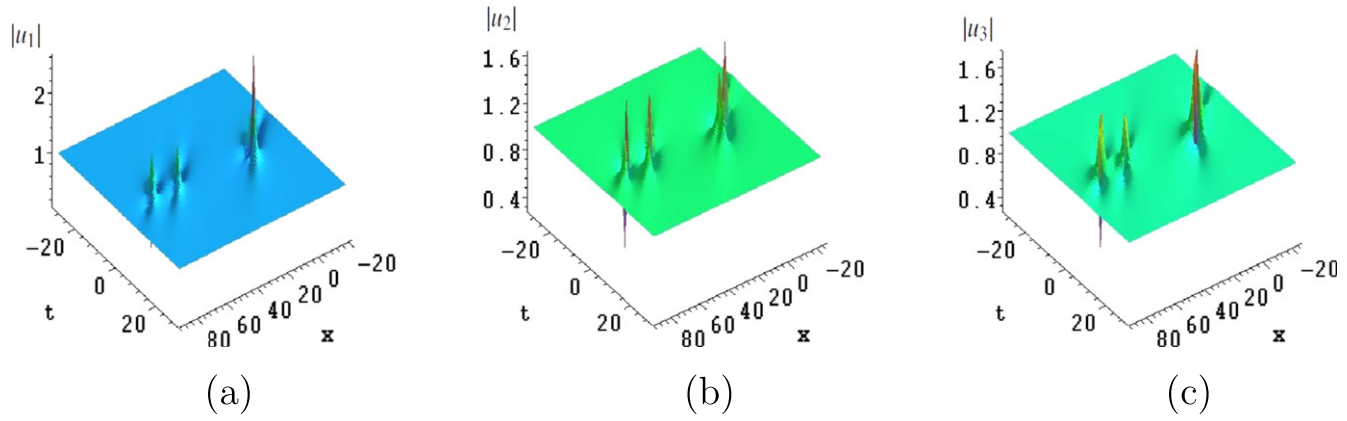

Figure 3. Evolution plot of the second-order rogue waves of line pattern 2 with $c_1 = 1, c_2 = 2, f_1 = 10, g_1 = 1, h_1 = 0, f_2 = 0, g_2 = 0, h_2 = 0$.

Table 1. Maximum amplitudes of the humps for four rogue waves coexisting case

Pattern	$\|u_1\|$	$\|u_2\|$
Line 1	3.1470, ($x = -0.0578$, $t = -1.0321$)	3.1470, ($x = 3.0385$, $t = 1.0321$)
Line 2	3.4080, ($x = 1.3510$, $t = 0.4339$)	3.4080, ($x = 0.0494$, $t = -0.4339$)
Fundamental	4.0324, ($x = 1.1246$, $t = 0.3180$)	4.0324, ($x = 0.1705$, $t = -0.3180$)
Pattern	$\|u_3\|$	
Line 1	3.0942, ($x = 0.5043$, $t = 0$)	
Line 2	3.0156, ($x = 2.4302$, $t = 0$)	
Fundamental	4.2037, ($x = 1.0750$, $t = 0$)	

equal to that in u_2 component, while in u_3 component the corresponding data is different. The detailed numerical values are shown in table 2; by putting $h_1 \neq 0$, $g_1 \neq 0$, the triangular pattern is obtained, see figures 6(a)–(c). Here, the new rogue wave is constituted by the interaction of four fundamental ones; by setting $h_1 \neq 0$, $g_2 \neq 0$, it is displayed that four fundamental rouge waves array with a parallelogram (quadrilateral pattern 1) in figures 7(a)–(c), and a new rogue wave which is formed by the interaction of two fundamental ones is localized in the interior of the parallelogram; by taking $h_1 \neq 0, f_1 \neq 0$, the dynamical structure is analogous to the above case except that the four fundamental rouge waves arrange with a trapezium (quadrilateral pattern 2), see figures 8(a)–(c); when by choosing $h_1 \neq 0, f_2 \neq 0$, we see that in figures 9(a)–(c), one fundamental rogue wave in the center along with five fundamental ones in the outer ring arranging with a circular pattern emerge on the temporal-spacial plane. Like the quadrilateral case, rogue waves over

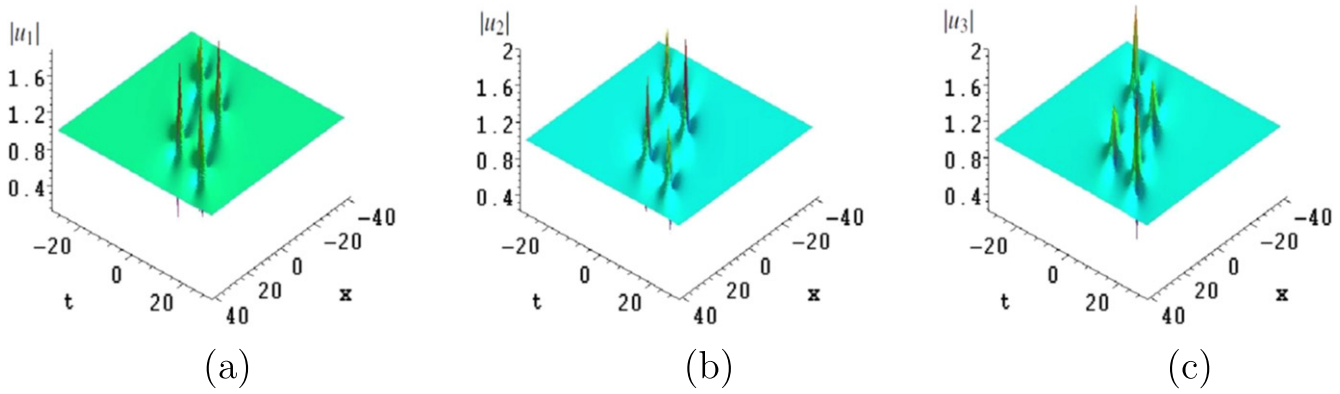

Figure 4. Evolution plot of the second-order rogue waves of quadrilateral pattern with $c_1 = 1$, $c_2 = 2$, $f_1 = 0$, $g_1 = 1$, $h_1 = 0$, $f_2 = 10\gtrdot 000$, $g_2 = 0$, $h_2 = 0$.

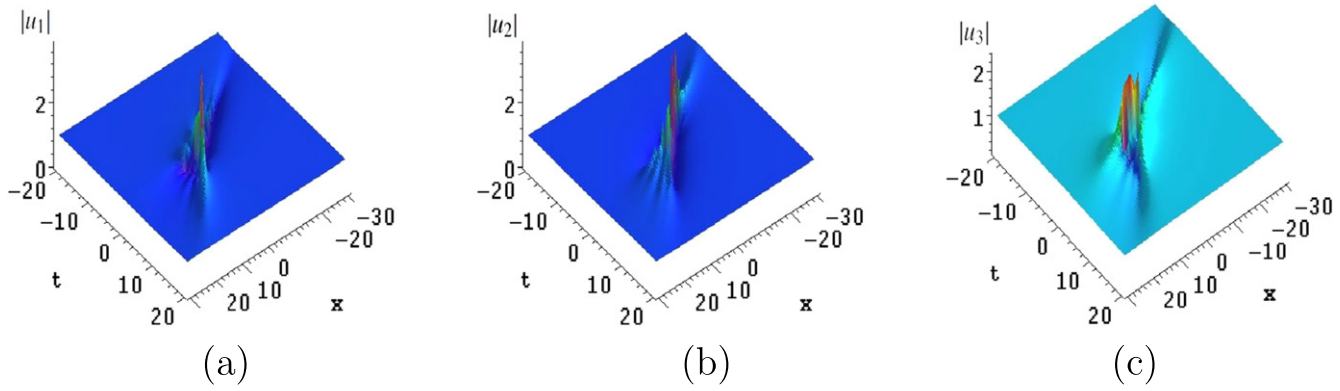

Figure 5. Evolution plot of the second-order rogue waves of fundamental pattern with $c_1 = 1$, $c_2 = 2$, $f_1 = 0$, $g_1 = 0$, $h_1 = 0.01$, $f_2 = 0$, $g_2 = 0$, $h_2 = 0$.

Table 2. Maximum amplitudes of the humps for six rogue waves coexisting case

Pattern	$\|u_1\|$	$\|u_2\|$
Quadrilateral 1	3.1416, ($x = -0.0302$, $t = -1.0048$)	3.1416, ($x = 2.9843$, $t = 1.0048$)
Quadrilateral 2	3.4201, ($x = 1.3444$, $t = 0.4326$)	3.4201, ($x = 0.0466$, $t = -0.4326$)
Triangular 2	4.0260, ($x = 1.1322$, $t = 0.3219$)	4.0260, ($x = 0.1664$, $t = -0.3219$)
Fundamental	4.7707, ($x = 1.0860$, $t = 0.3937$)	4.7707, ($x = -0.0950$, $t = -0.3937$)
Pattern	$\|u_3\|$	
Quadrilateral 1	3.1129, ($x = 0.5037$, $t = 0$)	
Quadrilateral 2	3.0119, ($x = 2.3871$, $t = 0$)	
Triangular	4.1362, ($x = 1.0745$, $t = 0$)	
Fundamental	5.5241, ($x = 2.0052$, $t = 0$)	

here are also tilted to a certain degree in the diagonal direction of the temporal-spacial plane comparing to that in the Manakov system.

4. Numerical simulations

In this section, we perform numerical simulations in the MATLAB platform to discuss stability problem of some higher-order rogue waves with different dynamics. Here, as is stated in the foregoing section, we assume x be the evolution variable in the present paper.

Firstly, we do numerical simulations to two special higher-order rogue waves with fundamental patterns, namely, the cases of four or six fundamental rogue waves completely merged with each other. The corresponding parameters are the same as that in figures 1 and 5, respectively. For the four fundamental rogue waves case, we set $x = -1$ as the initial value and the finite computational region of t be $[-10, 10]$ for $x \geqslant -1$. Considering the background wave function of the

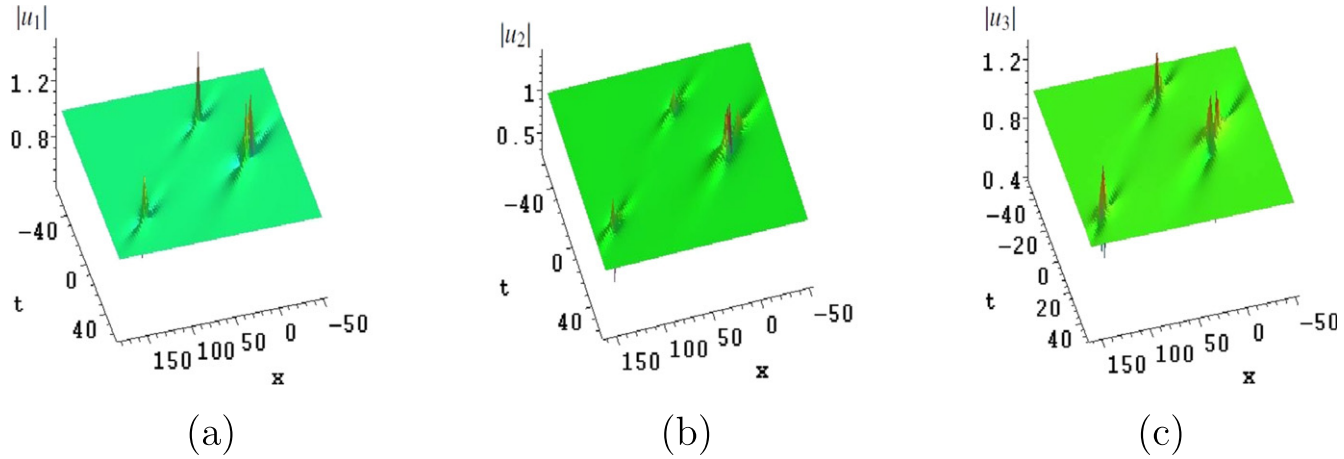

Figure 6. Evolution plot of the second-order rogue waves of triangular pattern with $c_1 = 1$, $c_2 = 2$, $f_1 = 0$, $g_1 = 1$, $h_1 = 0.01$, $f_2 = 0$, $g_2 = 0$, $h_2 = 0$.

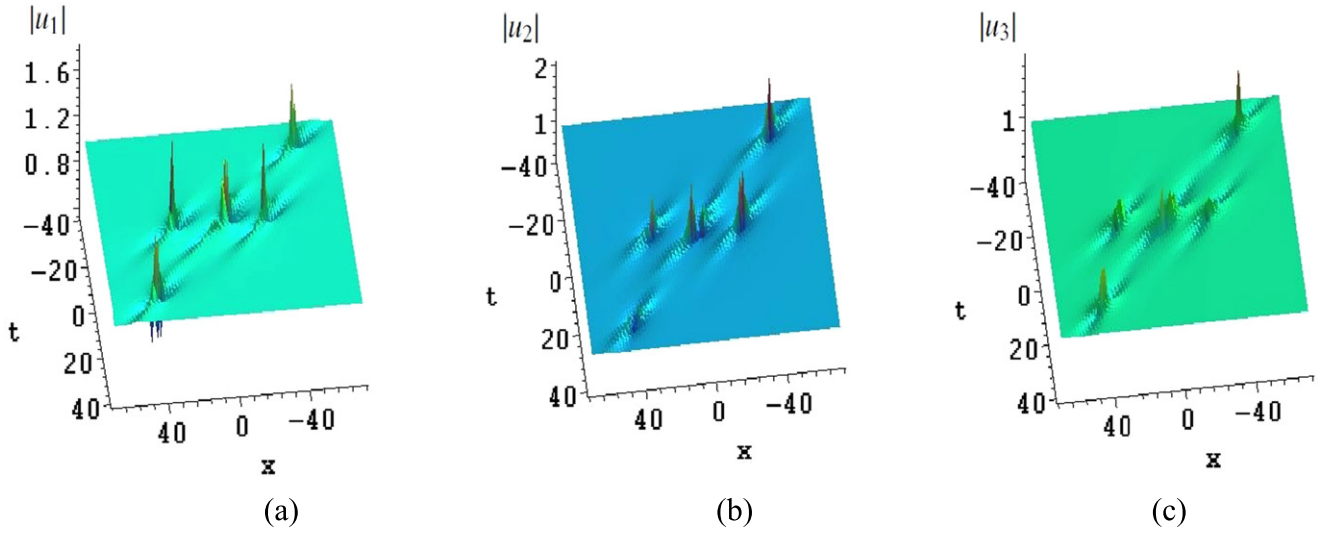

Figure 7. Evolution plot of the second-order rogue waves of quadrilateral pattern 1 with $c_1 = 1$, $c_2 = 2$, $f_1 = 0$, $vg_1 = 0$, $h_1 = 0.01$,$v f_2 = 0$, $g_2 = 1000$, $h_2 = 0$.

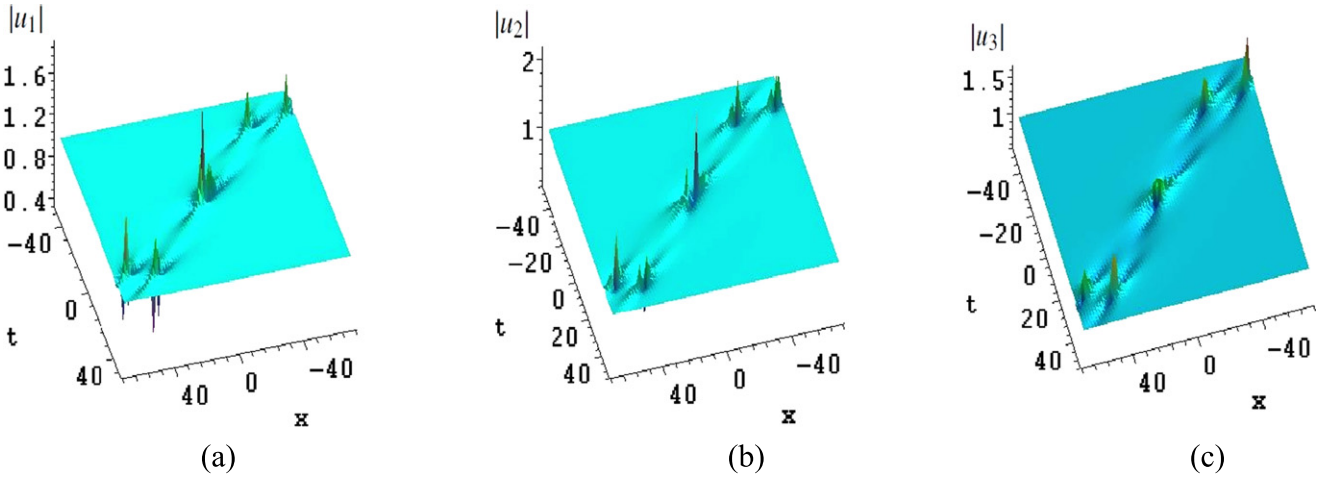

Figure 8. Evolution plot of the second-order rogue waves of quadrilateral pattern 2 with $c_1 = 1$, $c_2 = 2$, $f_1 = 10$, $g_1 = 0$, $h_1 = 0.01$, $f_2 = 0$, $g_2 = 0$, $h_2 = 0$.

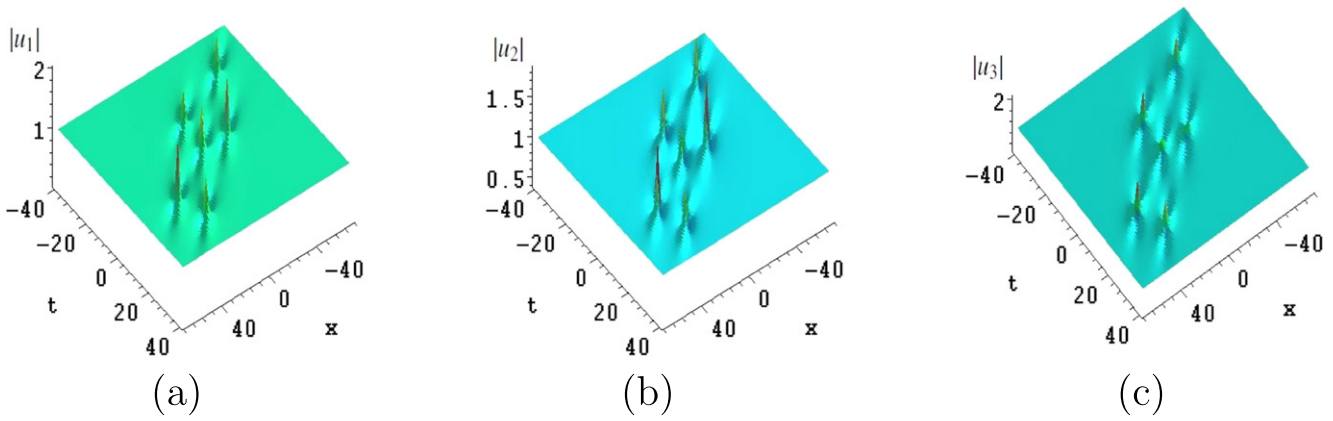

Figure 9. Evolution plot of the second-order rogue waves of circular pattern with $c_1 = 1$, $c_2 = 2$, $f_1 = 0$, $g_1 = 0$, $h_1 = 0.01$, $f_2 = 10000$, $g_2 = 0$, $h_2 = 0$.

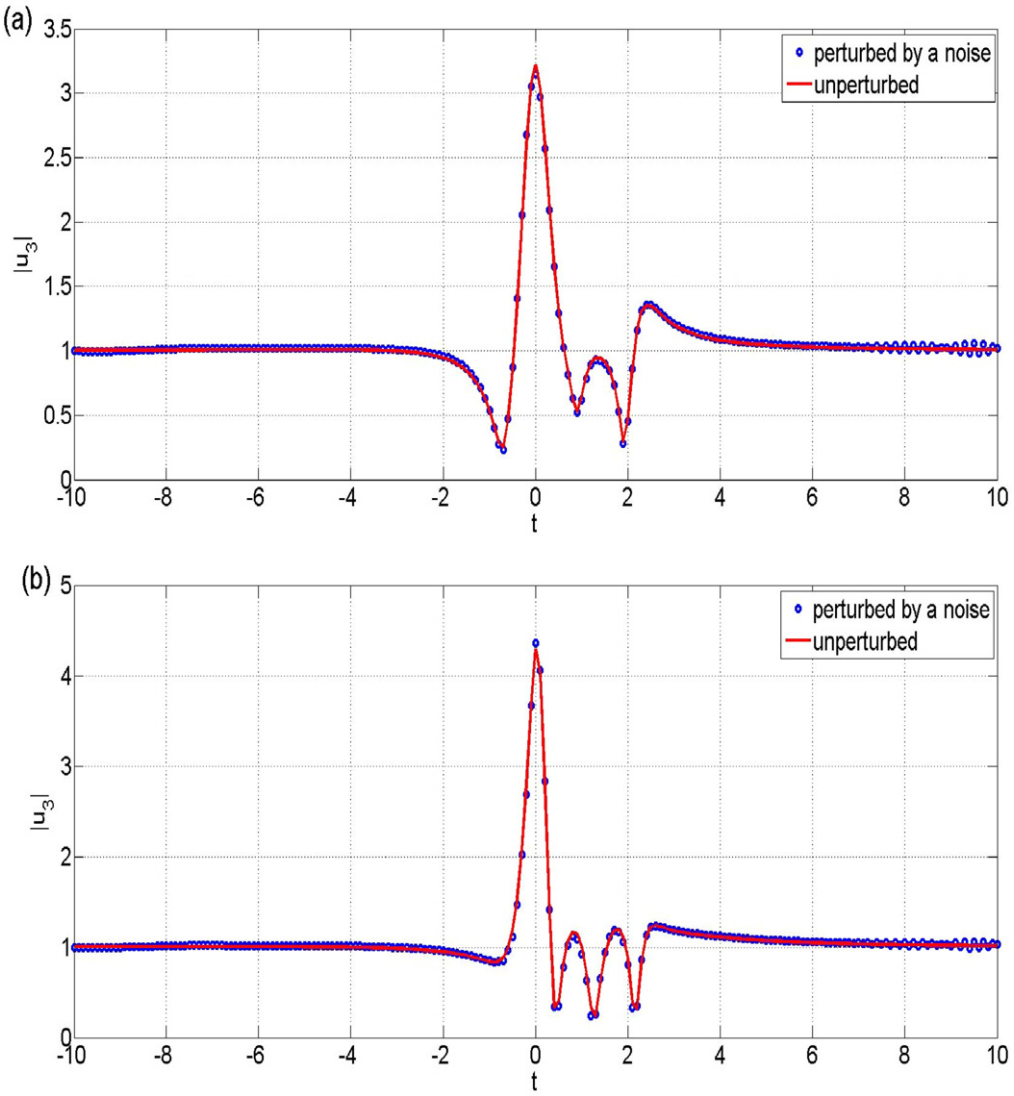

Figure 10. Numerical simulations of the higher-order rogue waves with fundamental patterns in u_3 component, (a) four fundamental rogue waves case at $x = 3$, the parameters are the same as that in figure 1; (b) six fundamental rogue waves case at $x = 3$, the parameters are the same as that in figure 5.

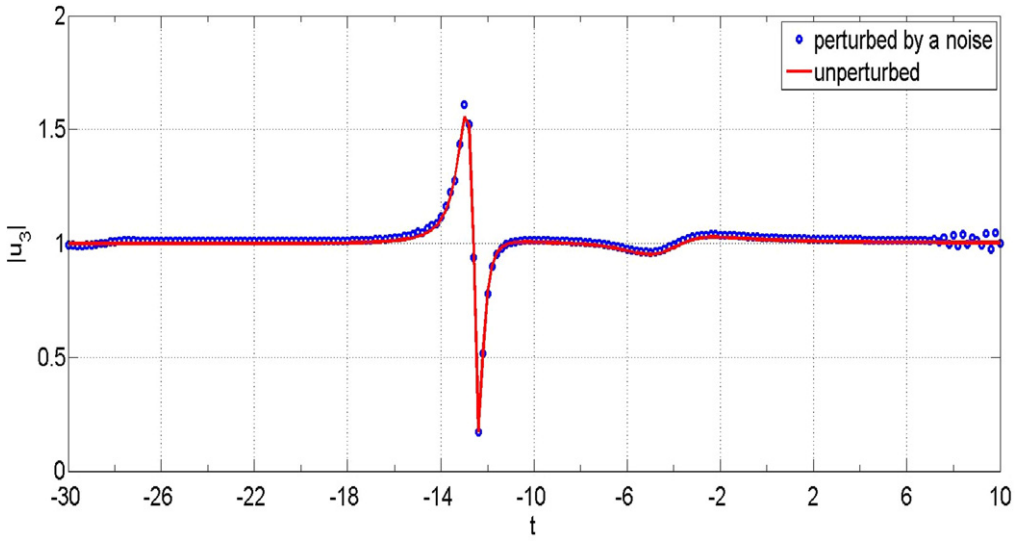

Figure 11. Numerical simulations of the higher-order rogue wave with quadrilateral pattern in u_3 component at $x = -18$, the parameters are the same as that in figure 4.

corresponding rogue wave solution derived by the determinant formulas, we choose the boundary condition be $u_1|_{t=\pm 10} = -\alpha_1 \exp[\mathrm{i}\theta_1]$, $u_2|_{t=\pm 10} = -\alpha_1^* \exp[\mathrm{i}\theta_2]$, $u_3|_{t=\pm 10} = \mathrm{i}\alpha_1 \exp[\mathrm{i}\theta_3]$, here $\alpha_1 = \exp[-\mathrm{i}\pi/3]$. Adding a 0.01 noise to the amplitude of the u_3 component, the numerical simulations of the evolution process at $x = 3$ can be shown in figure 10(a). We find that a small oscillation arises in the right boundary if the explicit solution is perturbed by a noise, while its shape and amplitude change slightly as the distance evolves. So, the higher-order rogue wave in this case can withstand the perturbation of the noise, and it has a stable propagation in the determined short computational interval. Similarly, the numerical simulations of the stable propagation for u_1 and u_2 components can also be obtained, here we refrain from presenting them. For the six fundamental rogue waves case, we choose the identical initial value, finite computational region and boundary condition, and adding a 0.01 noise to the amplitude of the u_3 component. We find that at $x = 3$ as shown in figure 10(b), there is also a small oscillation in the right boundary when a noise is added, while the basic shape and the amplitude of the rogue wave have almost no changes. So, in this case, the higher-order rogue wave can also bear the perturbation of the noise, and it can be seen as the stable propagation in the selective computational interval.

Secondly, we perform numerical simulations to one higher-order rogue wave with quadrilateral pattern, which is featured with four fundamental rogue waves well separated, and the corresponding parameters are the same as that in figure 4. Now we take $x = -22$ as the initial value and the finite computational region of t be $[-30, 10]$ for $x \geqslant -22$. By choosing the same boundary condition i.e. the background wave function of the corresponding rogue wave solution and the equal step length ratio in the computational process, the numerical simulations of the evolution process at $x = -18$ can be shown in figure 11. We present that when a 0.01 noise is added to the amplitude of the u_3 component, a clearer oscillation occurs at the right boundary and the point of the maximum amplitude. The higher-order rogue wave in this case can not withstand the perturbation of the 0.01 noise, and here the stability of the higher-order rogue waves with quadrilateral pattern is weaker than that of the fundamental patterns.

5. Conclusion

In summary, we investigate higher-order rogue wave solutions of the TWRI equation which serves as a basic model to describe the propagation and mixing of waves with different frequencies in weakly nonlinear dispersive media. By means of the generalized DT, a general Nth-order rogue wave solution on a special plane background with the same spectral parameter $\zeta_1 = \frac{3}{4}\sqrt{3}\,\mathrm{i}$ is derived. We present that the general solution comprises two characteristic velocities structural parameters c_1 and c_2 and $3N$ independent parameters f_k, g_k, h_k $(1 \leqslant k \leqslant N)$. As an application, we present a series of interesting dynamics of rogue waves by choosing different parameters. Moreover, the stability problem of some special rogue waves is discussed.

In addition, it is notable to say that the stability analysis and experimental observation of higher-order rogue waves in a coupled system is still an intractable problem due to its complexity and diversity, although some experimental data analysis and possibilities of existence for higher-order rogue waves in the Manakov system have been investigated [13, 14]. The stability analysis of the other interesting types of rogue waves presented in this paper (such as the triangular pattern, etc) deserves further investigation, and we hope the general rogue wave solutions and dynamical structures given here may contribute to better apprehending the complex extreme wave phenomena in nonlinear optics, plasma physics, fluid dynamics and so on.

Acknowledgments

The authors are greatly indebted to the editor and reviewer for their helpful comments and constructive suggestions, and one of the authors Xin Wang is grateful for Professor Yuqi Li's valuable discussion and help. The project is supported by National Natural Science Foundation of China (Grant Nos. 11275072 and 11435005), the Global Change Research Program of China (No. 2015CB953904), Research Fund for the Doctoral Program of Higher Education of China (No. 20120076110024), The Network Information Physics Calculation of basic research innovation research group of China (Grant No. 61321064), Shanghai Collaborative Innovation Center of Trustworthy Software for Internet of Things (Grant No. ZF1213), Shanghai Minhang District talents of high level scientific research project, Talent Fund and KC Wong Magna Fund in Ningbo University, National Natural Science Foundation of China (Grant No. 14BGL153), Henan Province young Key Teacher Project (Grant No. 2009GGJS-060), The twelfth five year plan project of Henan Province (Grant No. [2012]-JKGHAB-0027).

References

[1] Dysthe K, Krogstad H E and Müller P 2008 Oceanic rogue waves *Annu. Rev. Fluid Mech.* **40** 287–310
[2] Solli D R, Ropers C, Koonath P and Jalali B 2007 Optical rogue waves *Nature* **450** 1054–7
[3] Soto-Crespo J M, Grelu P and Akhmediev N 2011 Dissipative rogue waves: extreme pulses generated by passively mode-locked lasers *Phys. Rev.* E **84** 016604
[4] Bludov Y V, Konotop V V and Akhmediev N 2010 Vector rogue waves in binary mixtures of Bose–Einstein condensates *Eur. Phys. J.: Spec. Top.* **185** 169–80
[5] Akhmediev N, Ankiewicz A and Taki M 2009 Waves that appear from nowhere and disappear without a trace *Phys. Lett.* A **373** 675–8
[6] Peregrine D H and Austral J 1983 Water waves, nonlinear Schrödinger equations and their solutions *Math. Soc. B: Appl. Math.* **25** 16–43
[7] Chabchoub A, Hoffmann N P and Akhmediev N 2011 Rogue wave observation in a water wave tank *Phys. Rev. Lett.* **106** 204502
[8] Kibler B, Fatome J, Finot C, Millot J *et al* 2010 The Peregrine soliton in nonlinear fibre optics *Nat. Phys.* **6** 790–5
[9] Baronio F, Degasperis A, Conforti M and Wabnitz S 2012 Solutions of the vector nonlinear Schrödinger equations: evidence for deterministic rogue waves *Phys. Rev. Lett.* **109** 044102
[10] Manakov S V 1973 On the theory of two-dimensional stationary self-focusing of electromagnetic waves *Zh. Eksp. Teor. Fiz.* **65** 505–16
[11] Zhao L C and Liu J 2012 Localized nonlinear waves in a two-mode nonlinear fiber *J. Opt. Soc. Am.* B **29** 3119–27
[12] Guo B L and Ling L M 2011 Rogue wave, breathers and bright-dark-Rogue solutions for the coupled Schrödinger equations *Chin. Phys. Lett.* **28** 110202
[13] Ling L M, Guo B L and Zhao L C 2014 High-order rogue waves in vector nonlinear Schrödinger equations *Phys. Rev.* E **89** 041201
[14] Zhao L C, Xin G G and Yang Z Y 2014 Rogue-wave pattern transition induced by relative frequency *Phys. Rev.* E **90** 022918
[15] Degasperis A, Conforti M, Baronio F and Wabnitz S 2006 Stable control of pulse speed in parametric three-wave solitons *Phys. Rev. Lett.* **97** 093901
[16] Degasperis A and Lombardo S 2013 Rational solitons of wave resonant-interaction models *Phys. Rev.* E **88** 052914
[17] Kaup D J, Reiman A and Bers A 1979 Space-time evolution of nonlinear three-wave interactions: I. Interaction in a homogeneous medium *Rev. Mod. Phys.* **51** 275
[18] Lamb K G 2007 Tidally generated near-resonant internal wave triads at a shelf break *Geophys. Res. Lett.* **34** L186071
[19] Franklin R N 1977 Microinstabilities in plasmas-non-linear effects *Rep. Prog. Phys.* **40** 1369
[20] Burlak G, Koshevaya S, Hayakawa M, Gutierrez-D E and Grimalsky V 2000 Acousto-optic solitons in fibers *Opt. Rev.* **7** 323–5
[21] Zhou Z X 1998 Nonlinear constraints and soliton solutions of 1 + 2-dimensional three-wave equation *J. Math. Phys.* **39** 986–97
[22] Wu Y T and Geng X G 1999 A finite-dimensional integrable system associated with the three wave interaction equations *J. Math. Phys.* **40** 3409–30
[23] He G L, Geng X G and Wu L H 2014 Algebro-geometric quasi-periodic solutions to the three-wave resonant interaction hierarchy *SIAM J. Math. Anal.* **46** 1348–84
[24] Conforti M, Baronio F and Degasperis A 2011 Modulational instability of dark solitons in three wave resonant interaction *Physica* D **240** 1362–9
[25] Baronio F, Conforti M, Degasperis A and Lombardo S 2013 Rogue waves emerging from the resonant interaction of three waves *Phys. Rev. Lett.* **111** 114101
[26] Chabchoub A, Hoffmann N, Onorato M, Slunyaev A, Sergeeva A, Pelinovsky E and Akhmediev N 2012 Observation of a hierarchy of up to fifth-order rogue waves in a water tank *Phys. Rev.* E **86** 056601
[27] Kedziora D J, Ankiewicz A and Akhmediev N 2013 Classifying the hierarchy of nonlinear-Schrödinger-equation rogue-wave solutions *Phys. Rev.* E **88** 013207
[28] Wang L H, Porsezian K and He J S 2013 Breather and rogue wave solutions of a generalized nonlinear Schrödinger equation *Phys. Rev.* E **87** 053202
[29] Cao C W and Cao J L 2007 An integrable (2+1)-dimensional Toda equation with two discrete variables *Phys. Lett.* A **365** 301–8
[30] Cao C W and Cao J L 2006 On an integrable (2+1) dimensional Korteweg–de Vries equation with a discrete variable *Nuovo Cimento* B **121** 675–87
[31] Dubard P, Gaillard P, Klein C and Matveev V B 2010 On multi-rogue wave solutions of the NLS equation and positon solutions of the KdV equation *Eur. Phys. J.: Spec. Top* **185** 247–58
[32] Guo B L, Ling L M and Liu Q P 2012 Nonlinear Schrödinger equation: generalized Darboux transformation and rogue wave solutions *Phys. Rev.* E **85** 026607
[33] Wang X, Li Y Q and Chen Y 2014 Generalized Darboux transformation and localized waves in coupled Hirota equations *Wave Motion* **51** 1149–60
[34] Wang X, Li Y Q, Huang F and Chen Y 2015 Rogue wave solutions of AB system *Commun. Nonlinear Sci. Numer. Simul.* **20** 434–42
[35] Wang X, Yang B, Chen Y and Yang Y Q 2014 Higher-order rogue wave solutions of the Kundu–Eckhaus equation *Phys. Scr.* **89** 095210
[36] Guo R, Hao R Q and Zhang L L 2013 Dynamic behaviors of the breather solutions for the AB system in fluid mechanics *Nonlinear Dyn.* **74** 701–09
[37] Wang L, Li X, Qi F H and Zhang L L 2015 Breather interactions and higher-order nonautonomous rogue waves

for the inhomogeneous nonlinear Schrödinger Maxwell–Bloch equations *Ann. Phys.* **359** 97–114
[38] Wazwaz A M 2006 Exact solutions for the fourth order nonlinear Schrodinger equations with a cubic and a power law nonlinearities *Math. Comput. Modelling* **43** 802–8
[39] Li B and Chen Y 2007 Symbolic computation and solitons of the nonlinear Schrödinger equation in inhomogeneous optical fiber media *Chaos Solitons Fractals* **33** 532–9
[40] Xu T and Xu X M Single- and double-hump femtosecond vector solitons in the coupled Sasa–Satsuma system *Phys. Rev.* E **87** 032913